A BK-channel-mediated feedback pathway links single-synapse activity with action potential sharpening in repetitive firing

Article (Published Version)

NEUROSCIENCE

A BK channel–mediated feedback pathway links single-synapse activity with action potential sharpening in repetitive firing

Matvey V. Roshchin[1], Mikhail E. Matlashov[2]*, Victor N. Ierusalimsky[1], Pavel M. Balaban[1], Vsevolod V. Belousov[2,3,4], György Kemenes[5†], Kevin Staras[5†‡], Evgeny S. Nikitin[1†‡]

Action potential shape is a major determinant of synaptic transmission, and mechanisms of spike tuning are therefore of key functional significance. We demonstrate that synaptic activity itself modulates future spikes in the same neuron via a rapid feedback pathway. Using Ca^{2+} imaging and targeted uncaging approaches in layer 5 neocortical pyramidal neurons, we show that the single spike–evoked Ca^{2+} rise occurring in one proximal bouton or first node of Ranvier drives a significant sharpening of subsequent action potentials recorded at the soma. This form of intrinsic modulation, mediated by the activation of large-conductance Ca^{2+}/voltage-dependent K^+ channels (BK channels), acts to maintain high-frequency firing and limit runaway spike broadening during repetitive firing, preventing an otherwise significant escalation of synaptic transmission. Our findings identify a novel short-term presynaptic plasticity mechanism that uses the activity history of a bouton or adjacent axonal site to dynamically tune ongoing signaling properties.

INTRODUCTION

The waveform of the presynaptic action potential (AP) has a significant influence on neurotransmitter release, and the mechanisms that contribute to the tuning of spike shape are therefore of key interest (*1*–*3*). In cortical neurons, AP duration is significantly influenced by the repolarization driven by activation of Kv1 potassium channels (*4*). However, these channels typically inactivate during slow oscillations (*4*) and are electrically down-regulated by subthreshold somatic depolarization (*5*), processes that favor the broadening of APs and the enhancement of transmitter release. As such, keeping AP waveform and downstream transmission in check during repetitive firing demands additional mechanisms.

Large-conductance Ca^{2+}-activated voltage-dependent K^+ channels (BK channels) are potential candidates for such a role. In layer 5 (L5) pyramidal neurons, BK channels are located in proximal axonal regions (*6*), close to the axon initial segment (AIS) where spike initiation occurs (*7*), and, like Kv1, contribute to the repolarization phase of APs (*1*, *8*). In view of their localization and Ca^{2+} sensitivity, these channels therefore appear well placed to act as conduits linking events occurring at synapses to the sites of AP generation (*9*). For example, AP-evoked Ca^{2+} rises that occur in synaptic boutons or axonal structures could potentially contribute to a transient activation of BK channels that, in turn, shapes the waveform of future spikes. Such a short-term feedback pathway would correlate synaptic activation and Ca^{2+} influx to ongoing AP expression and ultimately downstream information transmission. Additionally, it would provide a mechanism to offset the consequences of activity history–dependent inactivation of Kv1 channels that might otherwise drive a significant escalation of transmission.

Here, we investigate this idea in L5 neocortical neurons, which are primary output cells with an already well-defined role in signal processing (*10*). Specifically, we used calcium imaging to characterize the spike-driven transient Ca^{2+} rises occurring at one of two defined axonal sites: the proximal bouton on the first collateral or the first node of Ranvier. We show that mimicking the activity-driven Ca^{2+} elevation at either of these regions using local uncaging is sufficient to bring about a significant sharpening of the AP waveform recorded at the soma, exclusively mediated by changes in repolarization velocity. Using local application of blockers, we demonstrate that this mechanism is specifically dependent on BK channel activity and plays a significant role in constraining AP broadening and maintaining high-frequency spiking in evoked bursts. Whole-cell paired recording approaches show that this spike modulation has downstream consequences for synaptic transmission, limiting the escalation of postsynaptic response amplitudes that would otherwise occur if AP broadening was not constrained. Our findings add significant new understanding to models of neuronal self-regulation, defining a mechanism where cells tune their own excitability and signaling properties according to their recent synaptic activity history.

RESULTS

Single spike–evoked Ca^{2+} rises in the first node of Ranvier and proximal bouton drive significant AP narrowing

To examine the idea that synaptically derived activity-driven Ca^{2+} rises might influence properties of AP expression, we focused our investigation on two defined axonal structures in rat L5 neurons in acute cortical slices. Specifically, these were the first node of Ranvier and the first synaptic bouton on the adjacent proximal collateral, both readily morphologically identifiable in neurons cotransfected with red fluorescent protein (TagRFP) and synaptophysin-SypHer-2 using a gene gun (Fig. 1A). As a starting point, we measured the

[1]Institute of Higher Nervous Activity and Neurophysiology, Moscow 117485, Russia. [2]Shemyakin-Ovchinnikov Institute of Bioorganic Chemistry, Russian Academy of Sciences, Moscow 117997, Russia. [3]Pirogov Russian National Research Medical University, Moscow 117997, Russia. [4]Institute for Cardiovascular Physiology, Georg August University Göttingen, D-37075 Göttingen, Germany. [5]Sussex Neuroscience, School of Life Sciences, University of Sussex, Brighton BN1 9QG, UK.
*Present address: Department of Anatomy and Structural Biology, Albert Einstein College of Medicine, 1300 Morris Park Avenue, Bronx, NY 10461, USA.
†Joint senior authors.
‡Corresponding author. Email: nikitin@ihna.ru (E.S.N.); k.staras@sussex.ac.uk (K.S.)

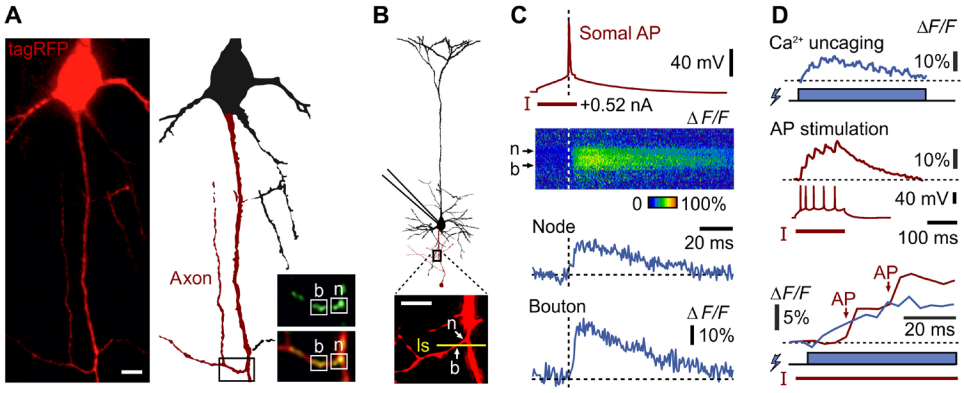

Fig. 1. Mimicking spike-evoked Ca^{2+} rises in presynaptic structures with targeted uncaging. (**A**) Confocal projection of target neuron expressing (left) tagRFP and (right) cartoon schematic. Inset shows green sypI-SypHer2 expression indicating target node ("n") and bouton ("b"). Scale bar, 10 μm. (**B**) Cartoon reconstruction of neuron used for imaging with Ca^{2+}-sensitive indicator OGB1. Bottom panel shows site of line scan (ls) (yellow) transecting the bouton and node. Scale bar, 10 μm. (**C**) Ca^{2+} transients in bouton and node evoked by a single AP. Pseudocolor plot (middle) and traces (bottom) of relative change in fluorescence (*ΔF/F*) for line scan in (b). (**D**) Ca^{2+} uncaging with DMNP-EDTA (top) evokes Ca^{2+} rise with equivalent amplitude to first AP in spike train (middle). Bottom: Detail of Ca^{2+} rises evoked by uncaging (blue) and APs (red) from above.

Ca^{2+} rise driven by evoked single somal spikes in whole-cell recordings by imaging with the fluorescence indicator Oregon Green 488 BAPTA 1 (OGB1) (Fig. 1, B and C). As expected, line scans revealed robust and transient Ca^{2+} increases that were comparable at both sites (Fig. 1C). Next, we used targeted uncaging with DMNP-EDTA (DM-Nitrophen) to mimic these Ca^{2+} increases and calibrated the response amplitude to single AP-driven events (Fig. 1D).

To test whether such a locally evoked Ca^{2+} rise alone could influence AP properties, we carried out experiments in which we uncaged Ca^{2+} and then, 20 ms later, elicited a spike using somal current injection. The uncaging was performed at one of four sites; the node, the proximal bouton, the cell exterior, or a dendritic region at the same distance from the soma (Fig. 2A). In each case, the morphological tracer Alexa Fluor 594 hydrazide was included in the patch-pipette solution to visualize neuronal structure. A further control used current-evoked AP generation without prior Ca^{2+} uncaging. Analysis of the normalized spike half widths revealed a striking effect of uncaging in the node or bouton versus all other conditions [Fig. 2, B and C; node, 90.1 ± 2.9%; bouton, 89.6 ± 2.7%; control, 100 ± 2.9%; no uncaging, 101.9 ± 2.6%; dendrite, 99.8 ± 2.8%; $^*P < 0.05$, $n = 5$, repeated-measures analysis of variance (ANOVA), pairwise Tukey's tests]. Specifically, we observed a significant narrowing of the AP (Fig. 2D) without a change in spike amplitude. We also observed a similar, albeit weaker effect when we locally uncaged at the second node of Ranvier (fig. S1). To rule out the possibility that the observed change in spike shape might be attributable to a nonspecific effect of the laser irradiation used for uncaging, we performed a further type of control experiment. L5 neurons ($n = 5$) were filled only with the Alexa dye and irradiated with the 405-nm laser to mimic the conditions of uncaging. We found no significant effect on AP half width of this laser irradiation (control before, 100 ± 1.5%; laser on node, 100 ± 1.5%; paired *t* test, $P = 0.9$). As an additional control that circumvented the Ca^{2+} uncaging approach altogether, we carried out experiments using targeted channelrhodopsin (ChR2) photostimulation to directly mimic spike-driven synaptic activation. Specifically, we used a transgenic mouse line to express ChR2 in L5 neurons and evoked somal spikes before and after local optogenetic stimulation of the bouton/node (fig. S2). In paired comparisons, we consistently observed a small but highly significant narrowing of the spike half width with bouton activation (ChR2 flashing, 97.6 ± 4.1%; control, 100 ± 4.2%; paired *t* test, $P < 0.01$, $n = 10$). This is particularly notable since the optogenetically driven subthreshold depolarization will inevitably also lead to Kv1 current inactivation that will drive AP broadening and thus limit the extent of this narrowing (*4*, *5*, *11*). Collectively, our findings strongly implicate a role for proximal synaptic or nodal activation, and the resulting Ca^{2+} rises, in contributing to accelerated recovery in the repolarization phase of a subsequent AP.

We reasoned that the spike narrowing we observe might be caused by diffusion of the uncaged Ca^{2+} to the AIS, where it could potentially activate BK channels. To test this possibility, we carried out experiments in which we imaged Ca^{2+} spread in the axon after the uncaging protocol. Specifically, we measured the amplitudes of Ca^{2+} transients in five axonal regions of interest (ROIs) (each ~15 μm in length) between the first node and the AIS (Fig. 2E). We found that while there was a significant Ca^{2+} transient in the node and its adjacent ROI neighbor, no responses above baseline level were seen at any other ROIs extending toward the AIS (Fig. 2F, left panel). By comparison, Ca^{2+} transients evoked by single somal spikes were similar in amplitude in each ROI (Fig. 2F, right panel). The effect of this nodally targeted uncaging is summarized in Fig. 2G, where a single exponential fit of the amplitude data shows a sharp distance-dependent decline, with negligible Ca^{2+} rises beyond the second ROI. Thus, the effect of the somatic AP narrowing is not attributable to Ca^{2+} diffusion into the AIS.

Synaptic activity–driven spike modulation is mediated by BK channels

We hypothesized that BK channels—Ca^{2+}-activated voltage-dependent K^+ channels with activation properties that are well suited to this form of intrinsic modulation (*12*)—might be possible mediators. To test this possibility, we used iberiotoxin (IbTx), a highly specific BK channel blocker, applied locally to the proximal bouton region (Fig. 3A and fig. S3). In the presence of IbTx, current-evoked single APs showed significant spike broadening compared to pre-IbTx application (Fig. 3B). To confirm this site specificity, we tested IbTx

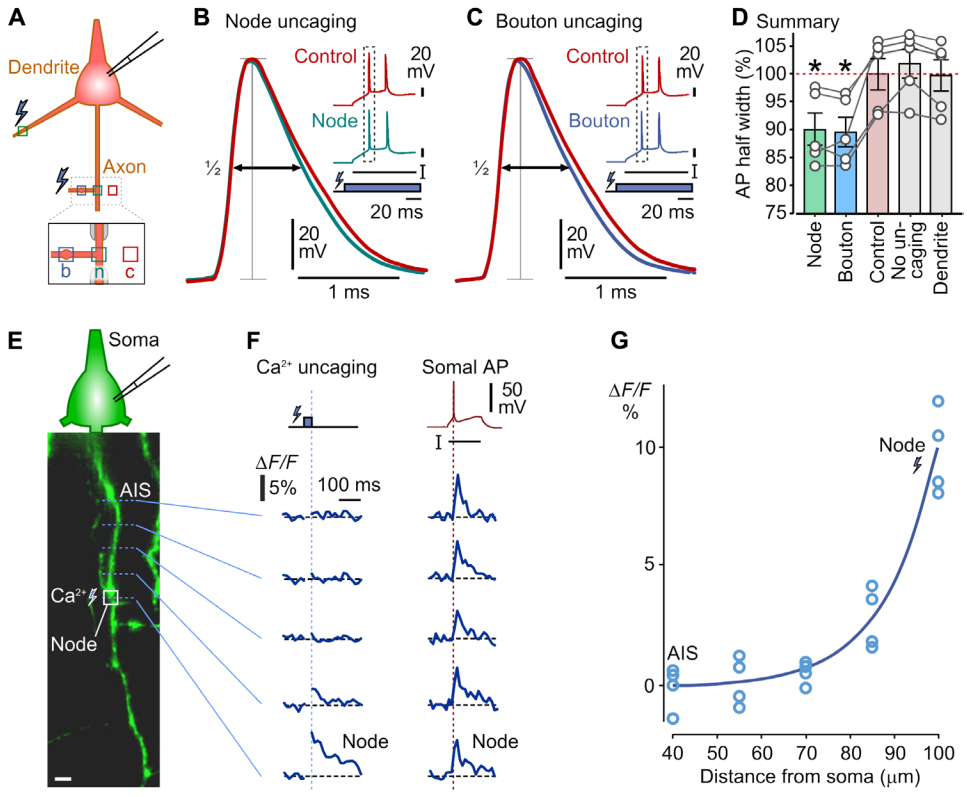

Fig. 2. Single spike–evoked Ca^{2+} rises in first node of Ranvier and proximal bouton drive AP narrowing. (**A**) Schematic for testing impact of Ca^{2+} uncaging on spike width showing uncaging targets (squares). (**B** and **C**) AP waveforms in neurons after uncaging at the node (B, green) or proximal bouton (C, blue) versus "external-to-neuron" control (red). Insets are compressed time scales of evoked spikes with uncaging and current injection indicated. (**D**) Mean ± SEM histogram for each condition. *$P < 0.05$ ($n = 5$, repeated-measures ANOVA, pairwise Tukey's tests). (**E**) Limited Ca^{2+} spread after targeted uncaging in the node. Image shows OGB2 fluorescence used for the readout of Ca^{2+} dynamics. (**F**) Left: Averaged traces (100-Hz acquisition) from ROIs (~15-μm length) along the axon during Ca^{2+} uncaging at the axonal node [white square in (E)]. Right: Somal AP–induced Ca^{2+} signals at same ROIs shown as a reference. (**G**) Plot summarizing Ca^{2+} signal propagation from the uncaging site in the node toward the AIS ($n = 4$ cells) at different ROIs. Each point shows the amplitude of uncaging-induced Ca^{2+} signal. A single exponential fit of the data (blue line) indicates that diffusion of uncaged Ca^{2+} from the node to the AIS was negligible.

applied at a dendritic site, ~150 μm from the bouton (Fig. 3C), and this revealed a significantly reduced influence on spike width (Fig. 3D; control axon, 100 ± 2.3%; axon, 122.9 ± 5.5%; control dendrite, 100 ± 3.4%; dendrite, 107 ± 2.4%, axon versus dendrite, $P < 0.05$, $n = 6$ for each, unpaired t test; see the figure legend for detailed statistics) consistent with a concentration dependence of IbTx action (fig. S3, A to D). Next, we examined whether IbTx would prevent the spike narrowing observed previously when Ca^{2+} was uncaged in the bouton (Fig. 3E). This proved to be the case; the spike half width elicited with Ca^{2+} uncaging and IbTx was indistinguishable from IbTx application alone (Fig. 3, E and F; control, 100 ± 3.9%; IbTx to bath, 125.8 ± 5.5%; IbTx + uncaging, 125.2 ± 5.5%; $P < 0.05$, $n = 6$, repeated-measures ANOVA, pairwise Tukey's tests). These findings strongly implicate BK channel function at presynaptic sites in contributing to this form of AP shaping.

As further confirmation of the involvement of BK channels, we examined the detailed kinetics of single-spike waveforms after uncaging. Since these channels are only known to influence the repolarization and after-hyperpolarization phases of APs (*1*, *9*), we hypothesized that the observed spike narrowing would be expected to arise from increases in repolarization speed alone. An analysis of spike velocity showed that this was the case (Fig. 4A; control, depolarizing phase: 100 ± 6% versus Ca^{2+} uncaging, depolarizing phase: 101.3 ± 5%, paired t test, $n = 7$, $P = 0.59$; control, repolarizing phase: 100 ± 4.7% versus Ca^{2+} uncaging, depolarizing phase: 112.2 ± 5.1%, $P < 0.01$, $n = 7$, paired t test). Next, we considered the pathway of action. We reasoned that modulation could arise from direct action of locally uncaged Ca^{2+} or alternatively through an extrinsic pathway activated by synaptic glutamate release. To differentiate between these possibilities, we applied a cocktail of ionotropic and metabotropic glutamate receptor blockers while uncaging Ca^{2+} in the bouton. Our results demonstrated that the presence of blockers had no impact on the Ca^{2+}-evoked reduction in spike half width (Fig. 4B; control, 100 ± 3.7%; cocktail, 99.8 ± 3.6%; cocktail + uncaging, 92 ± 3.8%; *$P < 0.05$, $n = 7$, repeated-measures ANOVA, pairwise Tukey's tests), indicating that this modulation is directly mediated and transmitter release–independent.

Given the well-established presence of BK channels in the AIS itself (*8*), we also investigated the effect of Ca^{2+} uncaging at this site on somal spike shape. As expected, uncaging led to a consistent narrowing of the AP (AIS uncaging, 96.6% ± 1.5%; control, 100 ± 1.7%; paired t test, $P < 0.01$, $n = 4$; fig. S4). Notably, however, the extent of this AIS-evoked narrowing was significantly less than observed with bouton uncaging, despite the more proximal position of the

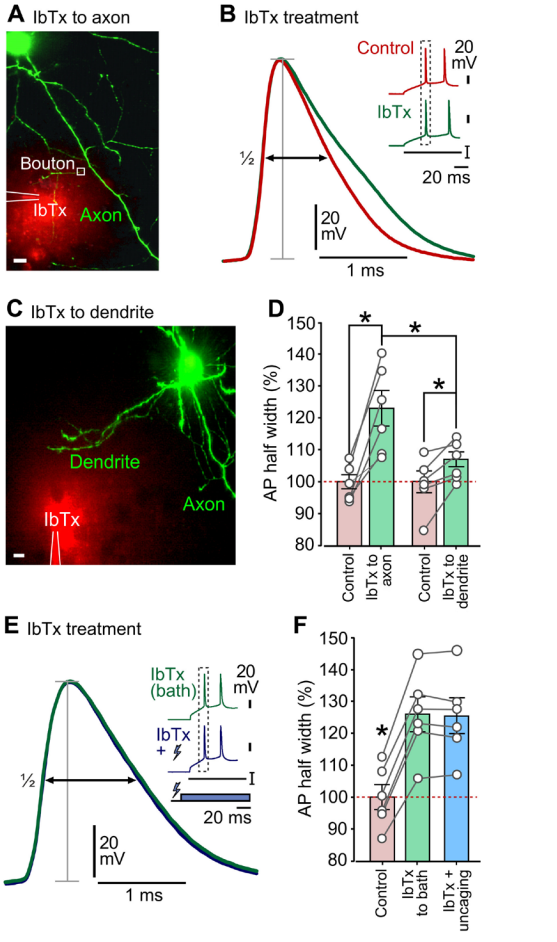

Fig. 3. Spike modulation is mediated by BK channels. (**A**) Example confocal projection showing local application of the BK channel blocker IbTx (red) to the first node and bouton region and (**B**) effect on AP width. Control is current-evoked spike alone. Scale bar, 10 μm. (**C**) Image shows alternative IbTx application site near dendrite and remote from bouton. Scale bar, 10 μm. (**D**) Summary histogram shows normalized AP half width versus pretreatment control spikes. Axon, $^*P < 0.01$ (paired *t* test, $n = 6$); dendrite, $^*P < 0.05$ (paired *t* test, $n = 6$); axon versus dendrite, $^*P < 0.05$ (unpaired *t* test, $n = 6$). (**E** and **F**) Traces and summary histograms reveal no Ca^{2+} uncaging-mediated spike narrowing in the presence of IbTx. $^*P < 0.05$ ($n = 6$, repeated-measures ANOVA, pairwise Tukey's tests).

AIS along the axon (AIS uncaging, 96.6% ± 1.5% versus bouton, 89.6 ± 2.7%; control, 100 ± 2.9%; unpaired *t* test, $P < 0.05$), suggesting that synaptic sites make the principal contribution to this form of spike modulation.

A further issue that we considered here was the specific relevance of BK channels in this mechanism versus the role of other conductances that contribute to the shaping of AP waveform, in particular Kv1. To test this, we carried out experiments in which we measured spike half widths in neurons that were continuously perfused with the Kv1 blocker 4-aminopyridine (4AP), before and after Ca^{2+} uncaging at the bouton (fig. S5). This revealed significant spike sharpening with bouton uncaging, even in the face of the substantial spike broadening associated with 4AP block (uncaging, 93.2 ± 12.1%; control, 100 ± 11.1%; $P < 0.05$, $n = 3$), consistent with our proposal that it is BK, not Kv1, channels that principally drive this effect.

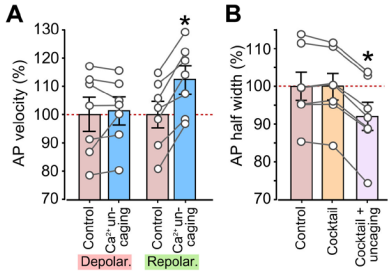

Fig. 4. Synaptic activation–driven spike modulation influences only the repolarization phase and does not depend on synaptic transmission. (**A**) Comparison of AP velocities of depolarization and repolarization measured at half peak for control current-evoked spike versus condition where current-evoked spike is preceded by Ca^{2+} uncaging. $^*P < 0.01$ ($n = 7$, paired *t* test). (**B**) Summary histogram of AP half widths for control current-evoked spike, current-evoked spike with cocktail of transmission blockers [6-cyano-7-nitroquinoxaline-2,3-dione (CNQX), 2-amino-5-phosphonopentanoate (AP5), α-methyl-4-carboxyphenylglycine (MCPG), and α-cyclopropyl-4-phosphonophenylglycine (CPPG)], and current-evoked spike with cocktail of transmission blockers preceded by Ca^{2+} uncaging. $^*P < 0.05$ ($n = 7$, repeated-measures ANOVA, pairwise Tukey's tests).

BK channel activity determines the extent of spike broadening in stimulus trains and maximizes firing in high-frequency bursts

Next, we examined how the observed spike modulation contributes to physiologically relevant ongoing activity. Given that BK channels contain high-affinity Ca^{2+}-binding sites (*13*), we reasoned that they might serve as key sensors of prior activity and that their activation could then play a potential role in limiting the extent of subsequent AP broadening that occurs during repetitive spiking. To examine this, we used a spike train protocol (Fig. 5A) in which we first generated a spike doublet to mimic the beginning of a high-frequency burst and then characterized the degree of AP broadening in a subsequent spike evoked at a variable interval after the initial train (Fig. 5, A and B). As expected, overall, we found a highly significant spike broadening as the intervals became shorter (Fig. 5B), but the half width values were strikingly variable across the recorded population of neurons at any given interval. We hypothesized that this might be due to differences in intrinsic BK channel function of individual cells. To test this directly, we obtained an index of BK channel function in each neuron by quantifying the degree of spike broadening in the presence of IbTx versus baseline, the assumption being that greater spike broadening in IbTx will indicate a higher basal level of BK channel activity. This experiment revealed a spread of basal BK channel index values ranging from 1.10 to 1.30 (Fig. 5C). Our prediction was that those neurons with the highest BK channel indices would show the narrowest APs at each interval in our spike train protocol. Consistent with this, when AP broadening was plotted against BK channel function at a given interval, it revealed a striking inverse correlation (Fig. 5D), and this was conserved across the full range of intervals tested as shown in a surface heatplot (Fig. 5E). These findings support a significant role for BK channel function in determining properties of the AP waveform during spike trains. We also hypothesized that this BK channel–driven repolarization might help facilitate high-frequency burst firing in these neurons, a role previously proposed in hippocampus (*14*). To test this, we used strong depolarizing current injection to drive a rapid spike train before and after IbTx treatment. We found that BK

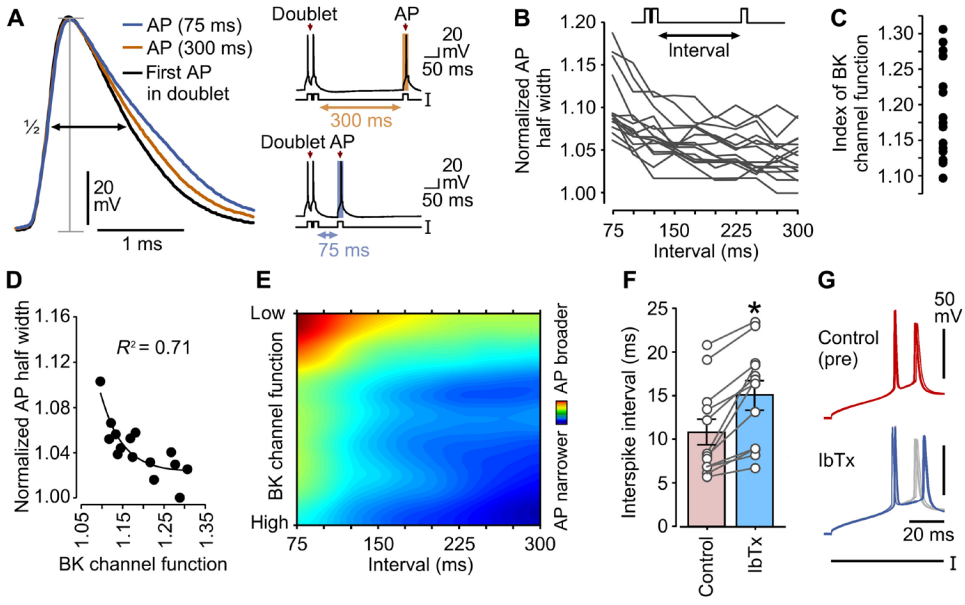

Fig. 5. BK channel activity constrains spike broadening in stimulus trains and supports high-frequency spiking. (**A**) Example traces showing that spike broadening varies with spike interval after evoked doublet (inset on right for intervals 300 and 75 ms) and (**B**) summary plot (n = 15 neurons, repeated-measures ANOVA, $P < 0.0001$). (**C**) Scatter plot showing that individual neurons have different intrinsic BK channel function based on an index quantifying the degree of spike broadening in the presence of IbTx versus baseline. (**D**) Scatter plot showing robust inverse relationship (one-phase exponential decay) when AP half width is plotted against BK channel function for a given interval (275 ms; goodness of fit, $R^2 = 0.71$; Spearman's correlation, −0.80; $P < 0.0003$; $n = 15$). (**E**) Surface plot showing relationship between BK channel function and spike broadening for all intervals tested (75 to 300 ms). (**F**) Histogram showing interval between first and second spikes in a depolarizing current-evoked burst in control and IbTx-treated neurons. *$P < 0.01$ (paired t test; $n = 12$). (**G**) Experimental example showing that IbTx applied locally to proximal bouton region (blue traces) extends interspike interval versus pretreatment controls (red and gray traces).

channel block resulted in a significant increase in the interspike interval, delaying the onset of the subsequent AP in a burst (control, 10.8 ± 1.5 ms; IbTx to bath, 15.1 ± 1.8 ms; paired t test, $P < 0.01$, n = 12; Fig. 5F). Moreover, the effect was even observable when we limited IbTx application to the proximal bouton region alone (Fig. 5G), suggesting that feedback from local synaptic activity, acting through a BK channel–mediated pathway, facilitates high-frequency firing.

Downstream information transmission is constrained by BK channel activation

We have shown that BK channel activation, driven by Ca^{2+} influx at single synaptic terminals, serves to constrain the AP broadening occurring during spike trains. Because our readout corresponds to the AP properties recorded at the soma, we next investigated the effects of BK channel block on signaling to target postsynaptic neurons using whole-cell patch-clamp recordings from monosynaptically connected cell pairs (Fig. 6A). Our aim here was to definitively test whether the changes observed in spike broadening corresponded to changes in synaptic efficacy associated with downstream information transmission. Specifically, we looked at the spike-evoked excitatory postsynaptic potentials (EPSPs) in a two-spike train, corresponding to a simple model of repetitive firing (Fig. 6B). As expected, compared to pretreatment control, IbTx induced a broadening in both APs, but the effect was significantly larger for the second spike (first AP, 121 ± 4%; second AP, 139 ± 10%; $P < 0.05$, $n = 12$, paired t test; Fig. 6C). Correspondingly, the second evoked EPSP was significantly larger under BK channel block (control, 0.64 ± 0.15 mV; IbTx, 0.94 ± 0.21 mV; $P < 0.05$, $n = 4$, paired t test; Fig. 6, D and E), driving a comparable increase in the paired-pulse ratio (control, 0.78 ± 0.18; IbTx to bath, 1.19 ± 0.05; $P < 0.05$, $n = 4$, paired t test; Fig. 6F). The increase in EPSP amplitude occurred in the absence of a change in pre- or postsynaptic somatic input resistance (103 ± 3% and 99 ± 2% of control, respectively; $P > 0.8$, $n = 4$, paired t test). Moreover, persistent increases in EPSP size after IbTx treatment could be seen in examples where a third spike was elicited in a train (Fig. 6C, inset). These findings suggest that the impact of BK channel activation serves to specifically limit the enhanced release that would otherwise be associated with runaway AP broadening during a spike train.

DISCUSSION

Here, we identify a BK channel–dependent feedback mechanism that links the activation of key axonal structures with the modulation of future AP shape. Using targeted Ca^{2+} uncaging approaches, we show that this modulation is significant even when single spike–driven Ca^{2+} elevations are imposed at the level of individual proximal boutons or nodes. In view of this, it seems likely that the activation of multiple synapses—as will occur when an AP invades the axonal arbor—would result in an even more marked spike modulation, consistent with the substantial levels of spike broadening we observed when the BK channel blocker IbTx was applied across a large axonal segment.

We show that this mechanism has particular relevance in the context of ongoing spike activity. Specifically, our findings indicate that the AP sharpening associated with synaptic activation contributes to a limiting of the spike broadening that accompanies AP expression in spike trains. In a simple model of repetitive firing, we found that neurons with higher intrinsic BK channel function tended to better resist spike broadening across varying intervals. We also demonstrate that BK channel activity has a frequency control function,

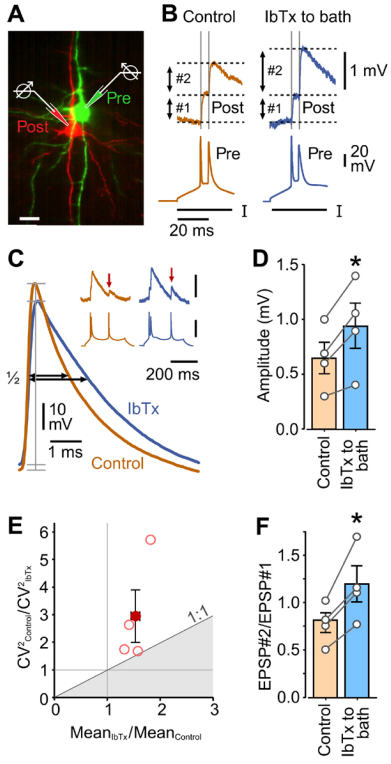

Fig. 6. Spike-evoked activation of BK channels limits ongoing synaptic release. (**A**) Experimental approach based on dual patch-clamp recording from monosynaptically connected L5 pyramidal neurons. Scale bar, 25 μm. (**B**) Typical traces showing EPSP responses to evoked spike pairs with 10-ms interspike interval for pretreatment control and post-IbTx. (**C**) Sample traces illustrate spike broadening effect of IbTx treatment on AP width for the second evoked spike. Inset: Example showing increased EPSP amplitude persists in the third spike–evoked response. Scale bars, 1 mV (top) and 50 mV (bottom). (**D** and **E**) Summary histogram of second EPSP amplitude (D) and coefficient of variation (CV) analysis for same data (E) plotted as the $CV^2_{Control}/CV^2_{IbTx}$ ratio against the mean amplitude ratio for IbTx versus control. Points lying above a 1:1 ratio signify a presynaptic change. Unfilled circles are individual cell pairs. Filled circle is mean ± SEM. (**F**) Histogram of EPSP#2-to-EPSP#1 amplitude ratio for pretreatment control and IbTx (*$P < 0.05$, paired *t* test, $n = 4$).

permitting higher-frequency firing in bursts than was achievable when BK channels were inhibited. It is already well established that the first node of Ranvier has a critical role in high-frequency burst generation in L5 axons (*15*), and our findings suggest that axonal BK channels contribute to this by facilitating membrane repolarization during repetitive firing. Moreover, this BK channel–activated spike modulation had direct consequences for downstream synaptic signaling, serving to limit transmission. Nonetheless, this effect was complex, with the attenuation of EPSP amplitude observed only for the second of a two-AP train. This implies that this regulatory feedback mechanism includes a delay, presumably because robust BK channel activation at the synapse depends on the calcium transient evoked by the first AP. This idea is highly consistent with our findings from the Ca^{2+} uncaging experiments, where prior Ca^{2+} elevation drives the narrowing of the subsequent spike. As such, this mechanism appears to be specifically tuned to limiting the enhanced transmission that would otherwise be associated with subsequent APs in an ongoing spike train.

Our findings here contrast with those of elegant previous work in hippocampal CA3-CA1 neurons showing that BK channels do not regulate transmitter release under basal conditions (*6*). Block of BK channel activity resulted in enhanced transmission only when Kv1 channels were first inhibited, implying that the BK channel–mediated brake on excessive signaling was perhaps only functionally relevant in specific pathological states where inactivation of Kv1 channels and Ca^{2+} accumulation occur (*6*). In granule cells projecting to CA3, Kv1 channels in mossy fibers inactivate rapidly but recover from inactivation very slowly, thus increasing AP-evoked Ca^{2+} entry into terminals particularly during long discharges (*16*). In our cortical study, BK channel function was pronounced even under conditions of minimal activation, calibrated to the Ca^{2+} rise measured with single evoked spikes, and this persisted with or without Kv1 block. These data suggest a difference in the basal functional role of BK channels in cortex versus hippocampus in contributing to spike shape modulation, perhaps reflecting additional demands in cortical cells for fine information processing associated with sensory discrimination. Whether more marginal rises in Ca^{2+} in cortical neurons might occur under certain conditions, influencing the relative contribution of Kv1 versus BK channel activity, is a key question for future work.

What is the nature of the signal that couples the changes in presynaptic and nodal waveform to the modulation of somal spike shape that we record? Our experiments rule out the possibility that the spread of Ca^{2+} itself to the AIS, where both nodal and somal spikes are generated, is directly responsible. A more likely mechanism is that modulation occurs through strong electrotonic coupling between these structures. Consistent with this, in L5 neurons, the soma and first node are linearly separated by only 100 to 150 μm, with the distance between the AIS and each of these structures being considerably shorter (50 to 75 μm). Evidence for a tight electrotonic coupling between the first node and AIS has already been reported (*4*, *15*), where whole-cell recordings reveal only a small (<10%) voltage attenuation across the first 150-μm axonal segment (*4*). As a result of this tight coupling, such AP-generated voltage changes spread rapidly from the AIS to both the first nodal region and the soma with a latency of 70 to 120 μs (*15*). It is therefore a reasonable expectation that local BK channel–mediated changes in AP shape will be reflected in similar changes in somal spikes.

A growing body of evidence suggests an important role of BK channels in short-term and long-term forms of activity-dependent regulation of intrinsic excitability (*17*, *18*). Our findings add further complexity to models of neuronal self-regulation, where cells adjust their own excitability according to their recent synaptic activity history. Given the central role of Ca^{2+} in use-dependent forms of short-term presynaptic plasticity (*19*–*21*), this mechanism represents a direct link between synaptic adaptation, intrinsic neuronal excitability, spike frequency determination, and downstream transmission. Modeling studies demonstrate that unidirectional homosynaptic plastic changes lead to runaway dynamics of synaptic weights (*22*). Thus, the regulatory mechanism described in our present work might play an important role in counterweighting Ca^{2+}-driven short-term homosynaptic facilitation with a Ca^{2+}-dependent negative feedback loop. The involvement of BK channels in this type of fast homoeostatic modulation is particularly significant in view of their established role in diverse functions, such as memory formation and seizure (*23*–*25*).

MATERIALS AND METHODS

Slice preparation

All experimental protocols were performed in accordance with the National Institutes of Health *Guide for the Care and Use of Laboratory Animals* and approved by the Department of Humanitarian Expertise and Bioethics of the Russian Academy of Sciences. Wistar rats (P19-24) of both sexes were deeply anesthetized with isoflurane and decapitated. Brains were rapidly removed and placed in ice-cold artificial cerebrospinal fluid (ACSF). Brain slices (350 μm) were cut using a vibratome (VT1200 S, Leica) from the primary visual cortex of the right hemisphere. ACSF contained 125 mM NaCl, 25 mM $NaHCO_3$, 27.5 mM glucose, 2.5 mM KCl, 1.25 mM NaH_2PO_4, 2 mM $CaCl_2$, and 1.5 mM $MgCl_2$ (all Sigma BioXtra–graded; pH 7.4) and aerated with 95% O_2 and 5% CO_2. The slices were incubated at room temperature for 90 min. Experiments commenced 120 min after slicing.

Patch-clamp recording

Patch pipettes (5 to 6 megohms) were filled with intracellular patch solution: 132 mM K-gluconate, 20 mM KCl, 4 mM Mg–adenosine triphosphate, 0.3 mM Na_2GTP, 10 mM Na-phosphocreatine, and 10 mM Hepes (pH 7.3) (all from Sigma). Brain slices were placed into a chamber continuously perfused with ACSF. Experiments were performed at or near physiological temperature (33° to 34°C) and visualized under differential interference contrast (DIC) infrared optics. Membrane potential was recorded in a whole-cell current clamp mode with an Axoclamp-2B amplifier and sampled at 20 to 50 kHz with the ADC (analog-to-digital converter) board Digidata 1440A under control of Clampex 10 software (all from Molecular Devices).

Confocal imaging and uncaging

Live-cell imaging was performed with an LSM 5 LIVE DuoScan confocal microscope (Zeiss) equipped with a chromatically corrected water immersion lens (Plan Apochromat IR DIC 63×, 1.0 NA, Zeiss). For recording, we selected L5 pyramidal neurons from visual cortex of young rats (P19-P22). Neurons were filled with the calcium-sensitive dye OGB1 (100 μM) by passive diffusion from the patch pipette for ~40 min. We imaged the bouton and node in the line scan mode (equivalent to imaging with a linear charge-coupled device) using a 488-nm laser and 505 long-pass (LP) emission filter at 300 to 500 lines/s. Alexa fluorescence was recorded with a 532-nm laser and 550 LP filter and subtracted from the baseline. The measured optical signal reflected the change in fluorescence relative to its mean value ($\Delta F/F$). For imaging of Ca^{2+} spread evoked by uncaging, we used OGB2 (100 μM). DMNP-EDTA (~5 mM; caged Ca^{2+}, Invitrogen) was loaded through the patch pipette by passive diffusion for ~40 min. This caged compound is reliably decomposed inside neurons using a 405-nm laser without neuronal damage (*26*). Neurons were deemed suitable for uncaging experiments only if they displayed the bouton and node in the same focal plane (±2 μm) at a depth of 15 to 30 μm from the slice surface. A square-shaped uncaging ROI was selected to encompass the target structure while minimizing the background region. The effectiveness of uncaging to increase the local axonal Ca^{2+} concentration was confirmed in experiments that combined uncaging and Ca^{2+} imaging with OGB1 (Fig. 1D). The morphological tracer Alexa Fluor 594 hydrazide (100 μM, Invitrogen) was added to the pipette solution for labeling of the recorded cells. After each imaging or uncaging experiment, we carefully removed the pipette by forming an outside-out patch and collected a fluorescence stack enabling three-dimensional reconstruction of the recorded neuron. We used the Alexa 594 signal to target relevant regions of the axon without photobleaching the OGB1 dye or inducing unwanted uncaging. To ensure the matching of the uncaging region with the target structures established with Alexa 594 imaging, we projected the 405-nm uncaging laser beam using a chromatically corrected lens and the same scanner used for imaging. With the 63× 1.0-NA objective, the optical resolution of the system was as follows: *z*, 1 μm; *x*, 0.44 μm; *y*, 0.44 μm.

Photostimulation with ChR2

Neurons of Thy1-ChR2-YFP transgenic mice were stimulated with a 488-nm laser line at ~0.3% of the nominal laser power of 200 mW. A square-shaped uncaging ROI was selected to encompass the target structure while minimizing the background region. The effectiveness of ChR2 activation was confirmed by minor but detectable subthreshold depolarizations in somatic recordings.

Gene gun transfection

Gold particles (1.6 μm) were coated with plasmids encoding tagRFP and the activity-sensitive presynaptic terminal marker Synaptophysin-SypHer-2 (sypI-SypHer2) (*27*) under a CMV promoter and attached to plastic tubing to make bullets. Freshly prepared brain slices were placed on paper filters and transfected with gold particles at 1.24 MPa followed by incubation at 35°C in ACSF with constant aeration for 6 to 8 hours.

Pharmacology

IbTx stock solution (Sigma, 100 μM), a BK channel antagonist, was dissolved in oxygenated ACSF and applied locally with positive pressure (55 kPa) using a patch pipette (tip concentration, 1 μM) positioned in the brain slice near the ROI. The pipette was positioned either adjacent to the axonal collateral (~40 μm from the first node) or close to a basal dendrite (~40 μm away and >150 μm from the first node). Alexa Fluor 594 hydrazide (red; 100 μM) was added to the pipette ACSF solution to visualize puffing. Neurons were labeled with Alexa Fluor 488 hydrazide (green, 100 μM) through the patch pipette. This application method allowed us to apply the drug rapidly and repeatedly without directly affecting ion channels in the apical dendrite. To estimate the concentration decay of IbTx at varying distances from a target structure (for example, axon or dendrite), we fitted the fluorescence of the puff (Alexa Fluor 594) with a single Boltzmann's curve (fig. S3, A to C). Calibration experiments demonstrated that at distances ≥110 μm, IbTx was not effective for >3 min. At distances ≤50 μm, IbTx application was effective at 1 min (fig. S3D). For some experiments, we used bath applications of agents [IbTx (0.05 μM), (+)MCPG (0.3 mM, Tocris), CNQX (5 μM, Sigma), and D-AP5 (20 μM, Sigma), CPPG (0.2 mM, Sigma), 4AP (0.2 mM)]. These were present for >10 min before testing their action. V_m averages for the recorded neurons were as follows: IbTx: control, −63.1 ± 0.9 mV; IbTx, −62.8 ± 1.4 mV; n = 6; Cocktail: control, −64.2 ± 0.7 mV; Glu blockers, −62.4 ± 0.6 mV; n = 7; Monosynaptic: control, −64.9 ± 1.7 mV; IbTx, −65.5 ± 1.6 mV; n = 4.

Dual-patch recording approach

Slices for dual patch were dissected in a modified ACSF (125 mM NaCl, 25 mM $NaHCO_3$, 27.5 mM glucose, 2.5 mM KCl, 1.25 mM NaH_2PO_4, 1 mM $CaCl_2$, and 3.5 mM $MgCl_2$) and incubated for 35 min at 34°C. For dual recording, a pair of Axoclamp-2B amplifiers

(Axon Instruments) (0.1 gain headstages) was used. The LN Bridge 500 slice chamber holder and two LN Junior (three axes) motorized manipulators were mounted on independent columns sitting on the LN V240 motorized shifting table (Luigs and Neumann). A target postsynaptic neuron was first patched in the whole-cell current clamp mode, and then, surrounding neurons were tested for synaptic connectivity using a high-resistance (10 to 12 megohms) pipette filled with 125 mM NaCl, 2.5 mM KCl, and 1.25 mM NaH_2PO_4 in loose-patch cell-attached configuration (50- to 100-megohm seal resistance). Test pulses (5 ms 3 to 5 nA) were used to identify connected pairs, after which the presynaptic neuron was repatched in the whole-cell mode with a conventional patch pipette (*28*). Each EPSP amplitude was measured in three to four trials and averaged.

Statistics

Histograms show means ± SEM. For statistical analysis, paired or unpaired *t* tests or ANOVA followed by post hoc tests was used.

SUPPLEMENTARY MATERIALS

Supplementary material for this article is available at http://advances.sciencemag.org/cgi/content/full/4/7/eaat1357/DC1

Fig. S1. Single spike–evoked Ca^{2+} rises in the second node of Ranvier drive AP narrowing.
Fig. S2. Photoactivation of the bouton/node with targeted ChR2 uncaging leads to significant spike narrowing.
Fig. S3. Determining parameters of IbTx application for local BK channel inhibition.
Fig. S4. Mimicking spike-evoked Ca^{2+} rises in distal AIS with targeted Ca^{2+} uncaging.
Fig. S5. Ca^{2+} uncaging at the bouton leads to significant spike narrowing in 4AP perfused neurons.

REFERENCES AND NOTES

1. B. P. Bean, The action potential in mammalian central neurons. *Nat. Rev. Neurosci.* **8**, 451–465 (2007).
2. M. B. Hoppa, G. Gouzer, M. Armbruster, T. A. Ryan, Control and plasticity of the presynaptic action potential waveform at small CNS nerve terminals. *Neuron* **84**, 778–789 (2014).
3. M. H. Kole, G. J. Stuart, Signal processing in the axon initial segment. *Neuron* **73**, 235–247 (2012).
4. M. H. Kole, J. J. Letzkus, G. J. Stuart, Axon initial segment Kv1 channels control axonal action potential waveform and synaptic efficacy. *Neuron* **55**, 633–647 (2007).
5. A. J. Foust, Y. Yu, M. Popovic, D. Zecevic, D. A. McCormick, Somatic membrane potential and Kv1 channels control spike repolarization in cortical axon collaterals and presynaptic boutons. *J. Neurosci.* **31**, 15490–15498 (2011).
6. H. Hu, L.-R. Shao, S. Chavoshy, N. Gu, M. Trieb, R. Behrens, P. Laake, O. Pongs, H. G. Knaus, O. P. Ottersen, J. F. Storm, Presynaptic Ca^{2+}-activated K^+ channels in glutamatergic hippocampal terminals and their role in spike repolarization and regulation of transmitter release. *J. Neurosci.* **21**, 9585–9597 (2001).
7. L. M. Palmer, G. J. Stuart, Site of action potential initiation in layer 5 pyramidal neurons. *J. Neurosci.* **26**, 1854–1863 (2006).
8. Y. Yu, C. Maureira, X. Liu, D. McCormick, P/Q and N channels control baseline and spike-triggered calcium levels in neocortical axons and synaptic boutons. *J. Neurosci.* **30**, 11858–11869 (2010).
9. C. Contet, S. P. Goulding, D. A. Kuljis, A. L. Barth, BK channels in the central nervous system. *Int. Rev. Neurobiol.* **128**, 281–342 (2016).
10. T. Bock, G. J. Stuart, The impact of BK channels on cellular excitability depends on their subcellular location. *Front. Cell. Neurosci.* **10**, 206 (2016).
11. Y. Shu, A. Hasenstaub, A. Duque, Y. Yu, D. A. McCormick, Modulation of intracortical synaptic potentials by presynaptic somatic membrane potential. *Nature* **441**, 761–765 (2006).
12. A. Pantazis, R. Olcese, Biophysics of BK channel gating. *Int. Rev. Neurobiol.* **128**, 1–49 (2016).
13. J. Cui, BK-type calcium-activated potassium channels: Coupling of metal ions and voltage sensing. *J. Physiol.* **588**, 4651–4658 (2010).
14. N. Gu, K. Vervaeke, J. F. Storm, BK potassium channels facilitate high-frequency firing and cause early spike frequency adaptation in rat CA1 hippocampal pyramidal cells. *J. Physiol.* **580**, 859–882 (2007).
15. M. H. P. Kole, First node of Ranvier facilitates high-frequency burst encoding. *Neuron* **71**, 671–682 (2011).
16. J. R. P. Geiger, P. Jonas, Dynamic control of presynaptic Ca^{2+} inflow by fast-inactivating K^+ channels in hippocampal mossy fiber boutons. *Neuron* **28**, 927–939 (2000).
17. A. B. Nelson, M. Faulstich, S. Moghadam, K. Onori, A. Meredith, S. du Lac, BK channels are required for multisensory plasticity in the oculomotor system. *Neuron* **93**, 211–220 (2017).
18. T. Zaman, C. De Oliveira, M. Smoka, C. Narla, M. O. Poulter, S. Schmid, BK channels mediate synaptic plasticity underlying habituation in rats. *J. Neurosci.* **37**, 4540–4551 (2017).
19. M. Blatow, A. Caputi, N. Burnashev, H. Monyer, A. Rozov, Ca^{2+} buffer saturation underlies paired pulse facilitation in calbindin-D28k-containing terminals. *Neuron* **38**, 79–88 (2003).
20. W. A. Catterall, A. P. Few, Calcium channel regulation and presynaptic plasticity. *Neuron* **59**, 882–901 (2008).
21. W. G. Regehr, Short-term presynaptic plasticity. *Cold Spring Harb. Perspect. Biol.* **4**, a005702 (2012).
22. J.-Y. Chen, P. Lonjers, C. M. Lee, M. Chistiakova, M. Volgushev, M. Bazhenov, Heterosynaptic plasticity prevents runaway synaptic dynamics. *J. Neurosci.* **33**, 15915–15929 (2013).
23. R. Brenner, Q. H. Chen, A. Vilaythong, G. M. Toney, J. L. Noebels, R. W. Aldrich, BK channel β4 subunit reduces dentate gyrus excitability and protects against temporal lobe seizures. *Nat. Neurosci.* **8**, 1752–1759 (2005).
24. E. A. Matthews, J. F. Disterhoft, Blocking the BK channel impedes acquisition of trace eyeblink conditioning. *Learn. Mem.* **16**, 106–109 (2009).
25. M. Typlt, M. Mirkowski, E. Azzopardi, L. Ruettiger, P. Ruth, S. Schmid, Mice with deficient BK channel function show impaired prepulse inhibition and spatial learning, but normal working and spatial reference memory. *PLOS ONE* **8**, e81270 (2013).
26. G. M. Billig, B. Pál, P. Fidzinski, T. J. Jentsch, Ca^{2+}-activated Cl^- currents are dispensable for olfaction. *Nat. Neurosci.* **14**, 763–769 (2011).
27. M. E. Matlashov, Y. A. Bogdanova, G. V. Ermakova, N. M. Mishina, Y. G. Ermakova, E. S. Nikitin, P. M. Balaban, S. Okabe, S. Lukyanov, G. Enikolopov, A. G. Zaraisky, V. V. Belousov, Fluorescent ratiometric pH indicator SypHer2: Applications in neuroscience and regenerative biology. *Biochim. Biophys. Acta* **1850**, 2318–2328 (2015).
28. D. Feldmeyer, G. Radnikow, Paired recordings from synaptically coupled neurones in acute neocortical slices, in *Advanced Patch-Clamp Analysis for Neuroscientists*, A. Korngreen, Ed. (Humana Press, 2016) p. 171–191.

Acknowledgments

Funding: This work was supported by the Russian Academy of Sciences and the Russian Foundation for Basic Research (16-04-00490 to E.S.N. and 17-00-00214 to V.V.B.), Russian Science Foundation (14-25-00072 to P.M.B.), Molecular and Cell Biology Program of Russian Academy of Sciences (to V.V.B.), and UK Biotechnology and Biological Sciences Research Council (BB/K019015/1 to K.S. and BB/H009906/1 to G.K.). **Author contributions:** E.S.N., K.S., and G.K. designed the study. M.V.R. and E.S.N. performed the experiments. E.S.N. performed the uncaging and dual-patch experiments. M.E.M. performed the gene gun experiments. V.N.I. contributed to the imaging experiments. K.S., P.M.B., G.K., E.S.N., V.N.I., M.V.R., and V.V.B. analyzed and discussed the data. K.S., E.S.N., and G.K. wrote the manuscript. **Competing interests:** The authors declare that they have no competing interests. **Data and materials availability:** All data needed to evaluate the conclusions in the paper are present in the paper and/or the Supplementary Materials. Additional data related to this paper may be requested from the authors.

Submitted 27 January 2018
Accepted 24 May 2018
Published 4 July 2018
10.1126/sciadv.aat1357

Citation: M. V. Roshchin, M. E. Matlashov, V. N. Ierusalimsky, P. M. Balaban, V. V. Belousov, G. Kemenes, K. Staras, E. S. Nikitin, A BK channel–mediated feedback pathway links single-synapse activity with action potential sharpening in repetitive firing. *Sci. Adv.* **4**, eaat1357 (2018).

ScienceAdvances

A BK channel–mediated feedback pathway links single-synapse activity with action potential sharpening in repetitive firing

Matvey V. Roshchin, Mikhail E. Matlashov, Victor N. Ierusalimsky, Pavel M. Balaban, Vsevolod V. Belousov, György Kemenes, Kevin Staras and Evgeny S. Nikitin

Sci Adv **4** (7), eaat1357.
DOI: 10.1126/sciadv.aat1357